Chinese Physics Letters **43**, 020714 (2026) **Express Letter**

Charge Excitations at Landau Level Crossings in WSe_2-Encapsulated Bilayer Graphene

Yuxuan Zhu[1], Zhecheng Li[2], Yixuan Xu[2], Yurong Ling[1], Zijun Lin[2], Zhimou Chen[1], Zhao Liu[2], Hailong Fu[2*], and Xi Lin[1,3,4*]

[1]*International Center for Quantum Materials, Peking University, Beijing 100871, China*
[2]*School of Physics, Zhejiang University, Hangzhou 310058, China*
[3]*Hefei National Laboratory, University of Science and Technology of China, Hefei 230088, China*
[4]*Interdisciplinary Institute of Light-Element Quantum Materials and Research Center for Light-Element Advanced Materials, Peking University, Beijing 100871, China*

(Received 11 December 2025; accepted manuscript online 15 January 2026)

Skyrmions—topological spin/pseudospin textures—are natural charge excitations of quantum Hall (QH) ferromagnets. In a WSe_2-encapsulated bilayer graphene (BLG) heterostructure, we tune the valley-only Landau level (LL) crossings at $\nu = \pm 3$ with an out-of-plane displacement field (D field) and use them as a platform to probe valley excitations. Activation gap measurements reveal a finite gap at degeneracy that rises sharply with D field near the crossing and exceeds the single-particle valley susceptibility, suggesting valley-skyrmion charge excitations. We quantify the skyrmion size and elucidate the mechanism governing its magnetic-field dependence. Similar behavior appears at valley-orbital and valley-spin entangled crossings ($\nu = \pm 2$ and $\nu = \pm 1$, respectively). These results suggest controlled valley-skyrmion formation in BLG and open a route to engineering interacting multicomponent QH ferromagnets with tunable spin/pseudospin textures.

DOI: 10.1088/0256-307X/43/2/020714 CSTR: 32039.14.0256-307X.43.2.020714

1. Introduction. Spin and valley degrees of freedom host the promise for achieving versatile electronic applications—such as low-consumption devices, memory technologies, and computation—in the post-Moore era.[1,2] Among the available excitations, skyrmions—smooth, topologically nontrivial spin/pseudospin textures—stand out as electrically addressable, nanoscale bits, which can be nucleated, driven, and read out by charge currents, gates, and microwave fields, providing robust functionality.[3–7] The quantum Hall (QH) ferromagnet offers a uniquely clean setting to realize and test skyrmions. Spin skyrmions have been extensively explored in GaAs quantum wells, in which exchange favors full spin polarization with small Zeeman energy and skyrmions appear as the lowest-energy charged excitations near integer fillings (notably $\nu = 1$).[8–13] Optically pumped nuclear magnetic resonance[8] and tilted-field transport measurements[9–11] quantified the number of flipped spins and the exchange activation gap. Complementary to spin, the valley degree of freedom is absent in GaAs systems (single Γ-valley conduction band), making it inaccessible to study valley skyrmions. By contrast, valley skyrmions have been observed in AlAs two-dimensional electron gas,[14–16] in which the valley degree of freedom has to be tuned by in-plane uniaxial strain aligned to the crystal axes; this approach demands careful calibration and dedicated hardware, and is therefore challenging to control. Graphene systems, hosting spin, valley, and orbital degrees of freedom and extensive QH states, are an ideal platform for exploring skyrmions. Indeed, spin skyrmions have been observed in graphene-based systems,[17–20] whereas studies of valley skyrmions remain comparatively scarce.[21]

Bilayer graphene (BLG) offers precise control of the valley degree of freedom. In the lowest Landau level (LLL), spin, valley, and orbital degeneracies form an eightfold manifold, while an out-of-plane displacement field (D field) acts as an effective layer/valley Zeeman field that can be swept continuously. This knob enables *in situ* tuning of valley polarization, selective preparation of pseudospin-ferromagnetic states, and controlled Landau level (LL) crossings between states of different quantum numbers.[22–26] Beyond electrostatic gating, van der Waals (vdW) heterostructures with proximitized graphene provide an atomic-scale platform for engineering band structure and interactions in the QH regime: proximity to adjacent materials modifies graphene's LL spectrum and internal symmetry breaking,[27–30] while the surrounding dielectric and gate geometry tune Coulomb interaction strength and screening, thereby controlling QH states and collective excitations.[31,32] Within these landscapes, BLG-based heterostructures, with their multicomponent LLL and electrically tunable band structure, are particularly well suited for exploring QH effect and its collective excitations.

In this Letter, we traverse valley-only LL crossings by tuning D field in a WSe_2/BLG/WSe_2 heterostructure and extract activation gaps from temperature-dependent transport around these crossings; we observe a finite gap

*Corresponding authors. Email: hailongfu@zju.edu.cn; xilin@pku.edu.cn
© 2026 Chinese Physical Society and IOP Publishing Ltd. All rights, including for text and data mining, AI training, and similar technologies, are reserved.

at the crossing, an initially steep growth of the energy gap with D field that exceeds the single-particle valley susceptibility, and a recovery of single-particle slope far from the crossing—together pointing to a valley-skyrmion picture. This establishes BLG-based vdW heterostructures as a clean and tunable platform for studying interaction-driven pseudospin textures.

2. Sample Characterization. Experimental measurements were performed on a WSe_2-encapsulated BLG device, a schematic of which is shown in Fig. 1(a). Here the WSe_2 layers on both sides not only induce proximity spin–orbit coupling (SOC) in BLG, but also serve as gate dielectrics. Independent control of the carrier density n and the out-of-plane D field is achieved with bottom and top graphite gates. The thin dielectrics (4.6 nm) and their relatively large dielectric constant (∼6.24) [33,34] produce strong screening effects from both themselves and the graphite gating layers to BLG. As a consequence, long-range Coulomb interactions are expected to be strongly suppressed and LL mixing should be weak in our device, which facilitates well-developed integer QH states with clearly resolved integer-state excitations. Four-terminal measurements on an etched Hall bar with Cr/Au contacts were carried out in a dilution refrigerator and a ^{3}He insert, using standard lock-in techniques at 17.43 Hz with a 1 nA AC excitation.

Figure 1(b) shows the longitudinal resistance R_{xx} versus D along the charge-neutrality line ($n = 0$) at $B = 0$ for temperatures from 2 K to 20 K. A central resistance peak at $D = 0$, flanked by two minima at $\pm D^*$, is resolved at low temperatures. This "peak-with-two-minima" structure is the expected transport signature of a closing and reopening of the band gap as D is swept, i.e., a transition between the band-inverted phase near $D = 0$ and the trivial band-insulating regime at large D field, consistent with prior calculations and experiments. [29,35] The positions of the minima $\pm D^*$ provide a direct estimate of the induced Ising SOC $|\lambda_I^T| = |\lambda_I^B| \approx 0.8$ meV in our sample [see Section III in the Supplementary Materials (SM)]. In the band-insulating regime, the D field enters the single-particle Hamiltonian as an interlayer potential difference u, which is proportional to D. As shown in the inset in Fig. 1(b), the band gap is analyzed via Arrhenius fits, and the data for $|D| > 10$ mV/nm on both sides yield an effective valley susceptibility $|g_D| \approx 1\,\mathrm{K(mV/nm)}^{-1}$, analogous to the result from previous work. [25]

Longitudinal resistance R_{xx} and Hall resistance R_{xy} were then mapped as functions of carrier density n and D field at different magnetic fields. An exemplary map of $R_{xx}(n, D)$ at $B = 4$ T and $T = 40$ mK is shown in Fig. 1(c). We observed well-developed QH states of the LLL and D-field-driven QH phase transitions at the same filling factors, which exhibit sharp R_{xx} spikes as a function of D field, signaling LL crossings. Figure 1(d) plots R_{xy}–D curves for $\nu = 2$ at different magnetic fields, illustrating B dependence of the crossing positions. Crossing positions versus B are summarized for each filling factor; representative results for $\nu = 1$, 2, 3 are plotted in Fig. 1(e) (see other filling factor results in Fig. S4 in the SM).

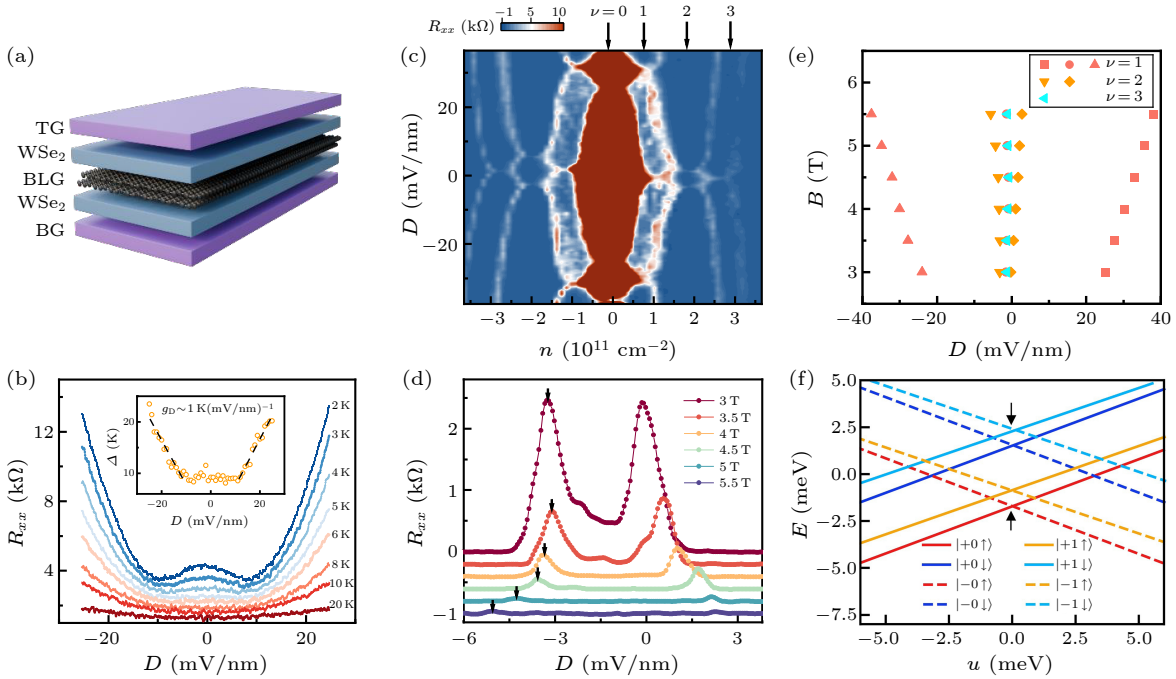

Fig. 1. (a) Schematic of the device. WSe_2 flakes (4.6 nm) encapsulate on both sides of the BLG and serve as the gate dielectrics. (b) Temperature dependence of the longitudinal resistance (R_{xx}) along the charge-neutrality line ($n = 0$) at $B = 0$ T. Inset shows the gap derived from Arrhenius fitting and g_D extracted from the slope. (c) Map of longitudinal resistance (R_{xx}) as functions of carrier density n and D field at $B = 4$ T and $T = 40$ mK. QH states and LL crossings of the LLL are shown in the map. (d) Traces of R_{xx} vs. D field around $\nu = 2$ crossings extracted from the map at different magnetic fields. Positions of the left crossings are marked by arrows in the plot. (e) Summary of the crossing positions for $\nu = 1$, 2, 3 as a function of B from 4 T to 5.5 T. (f) Calculated energy spectrum of the LLL with proximity-induced Ising SOC ($\lambda_I^T = 0.8$ meV, $\lambda_I^B = -0.8$ meV) at finite B. The arrows indicate the $\nu = \pm 3$ crossings, where valley flips occur while spin and orbital indices remain unchanged.

By analyzing the D field positions of the LL crossings, and using a single-particle BLG model with proximity-induced Ising SOC (see Section III in the SM), we determine the spectrum of the eight sublevels of the LLL labeled by (ξ, n, σ), where $\xi = +, -$, $n = 0, 1$ and $\sigma = \uparrow, \downarrow$ denote valley, orbital, and spin degeneracies respectively. An exemplary calculated energy-level diagram in a finite magnetic field with Ising SOC ($\lambda_{\mathrm{I}}^{\mathrm{T}} = 0.8\,\mathrm{meV}$, $\lambda_{\mathrm{I}}^{\mathrm{B}} = -0.8\,\mathrm{meV}$) is shown in Fig. 1(f), from which we identify the species nature of the level crossings. In particular, the crossings at $\nu = \pm 3$ involve valley flips driven by the effective D field, while spin and orbital quantum numbers remain unchanged, providing a clean setting to probe valley excitations. The $\nu = \pm 3$ valley-only crossings therefore serve as the primary focus in the following discussion.

3. Result and discussion. To further understand the underlying physics at the LL crossings and explore valley excitations, R_{xx} was measured as a function of D field across each crossing over a range of temperatures to examine thermally activated behavior. At $B = 8\,\mathrm{T}$, the resistance magnitude associated with the $\nu = \pm 3$ and $\nu = \pm 2$ crossings increases as a function of temperature with D-field-dependent starting points that indicate varying energy gaps at different D fields. As an example, figure 2(a) shows the resistance evolution of $\nu = 3$. Activation gaps Δ are extracted by fitting $R_{xx}(T)$ at fixed D field to an Arrhenius form $R_{xx} \propto \mathrm{e}^{-\Delta/2k_{\mathrm{B}}T}$. Figure 2(b) displays Arrhenius plots of R_{xx} at several D field values [regions I to V in Fig. 2(a)], and the resulting energy gap as a function of D field at the $\nu = 3$ crossing is summarized in Fig. 2(c). In addition, the resistance spikes are absent at $T = 40\,\mathrm{mK}$ and reappear around $T \approx 150\,\mathrm{mK}$ (see Fig. S3 in SM). The disappearance of the resistance spike is a direct and natural consequence of a finite charge gap and the restoration of an incompressible QH state.

Before discussing the D-field-dependent energy gap in detail, we outline the expected valley-splitting structure at $\nu = 3$ in a single-particle, non-interacting picture. Analogous to Zeeman-driven spin splitting ($E_{\mathrm{z}} = g_b \mu_{\mathrm{B}} B$, where $g_b = 2$), the single-particle valley splitting can be parameterized as $E_{\mathrm{v}} = g_{\mathrm{D}} \delta D$ ($|g_{\mathrm{D}}| \approx 1\,\mathrm{K(mV/nm)}^{-1}$ as discussed above and $\delta D = D - D_0$ where D_0 is the position of crossing). In this picture, the level crossing at $D = D_0$ is a first-order transition between oppositely valley-polarized states: the gap vanishes at D_0 and grows linearly with δD with slope g_{D}, plotted as grey dashed lines in Fig. 2(c). The measured energy gap Δ at $\nu = 3$ exhibits a steep minimum around the crossing point yet remains a finite gap at the level degeneracy. This behavior is consistent with the sharp resistance spike at the crossing above 150 mK and with its eventual disappearance at low temperature. Intriguingly, there is an essential discrepancy between the measured energy gap and the prediction of the single-particle, non-interacting picture described above.

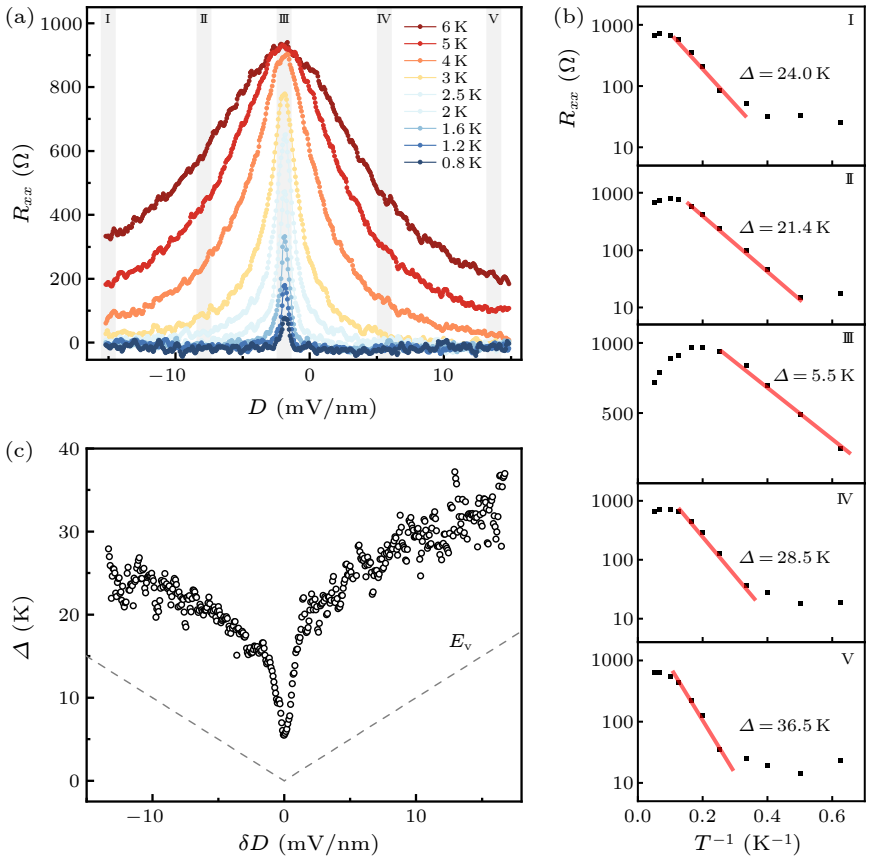

Fig. 2. (a) Temperature dependence of R_{xx} across the $\nu = 3$ crossing at $B = 8\,\mathrm{T}$. (b) Arrhenius plots of R_{xx} at the shaded positions (I to V) in (a). The red lines show the Arrhenius fits for the data. The resistance spike at the crossing also exhibits thermally activated behavior and yields a finite gap. (c) Activation gap Δ vs. δD. The grey dashed line represents the single-particle and non-interacting valley splitting energy E_{v}. The energy gap shows a steep minimum at the crossing and strong deviation from the ideal prediction.

Three features are particularly noteworthy: (i) the finite gap at the crossing contrasts with the non-interacting picture; (ii) near the crossing, the energy gap increases with δD much faster than $E_{\rm v}$; (iii) far from the crossing, the gap varies with δD with the same slope as $E_{\rm v}$, consistent with the single-particle limit. Taken together, these observations indicate many-body charge excitations between pseudospin-degenerate levels. More specifically, the experimental results are highly consistent with valley-skyrmion excitations at the $\nu = 3$ crossing, where the valley index flips while the spin and orbital quantum numbers remain unchanged.

The behavior can be interpreted within a framework which has been extensively applied to spin skyrmions in GaAs[9] and subsequently adapted to valley skyrmions in AlAs[14,15] in past works. In a Zeeman-split spin QH ferromagnet (e.g., $\nu = 1$ in GaAs quantum wells), $\eta = E_{\rm z}/E_{\rm c}$ is introduced to characterize charge-excitation behavior, where $E_{\rm z}$ is the Zeeman energy and $E_{\rm c}$ is the Coulomb energy in the sample. Even at zero Zeeman energy ($\eta = 0$), the ground state exhibits a finite gap equal to a fraction of the Coulomb energy ($\approx 0.63E_{\rm c}$).[11,36,37] The interaction-induced gap increases rapidly with η and the slope $\partial\Delta/\partial E_{\rm z}$ gives the number of flipped spins per charge excitation, i.e., skyrmion size directly. This slope decreases gradually and reverts to one beyond a critical value of $\eta(\approx 0.054)$,[36] indicating that charge excitation returns to the single-particle picture. Phenomenologically, this evolution reflects the competition between $E_{\rm z}$ and $E_{\rm c}$: at small $E_{\rm z}$, it is energetically favorable to distribute the reversed spin over many electrons, forming a large spin texture and preserving exchange correlations, whereas increasing $E_{\rm z}$ penalizes each flipped spin and drives the optimal charged excitation toward a single-flip quasiparticle. For valley textures, in the absence of explicit microscopic calculations, prior works in AlAs adopt a direct spin-skyrmions analogy by redefining $\eta = E_{\rm v}/E_{\rm c}$, with the skyrmion size obtained from the near-crossing slope $\partial\Delta/\partial E_{\rm v}$.[14,15] For $\nu = \pm 3$ valley-only crossings in our sample, the valley degree of freedom forms an $SU(2)$ pseudospin, closely analogous to that in the AlAs system, making the universal skyrmion framework applicable to our system.

With the valley skyrmion interpretation for $\nu = 3$ crossing in the present system, the valley skyrmion size is characterized by $s \equiv (\partial\Delta/\partial E_{\rm v})_{\eta\to 0}$. Physically, s quantifies the number of valley flips participating in the lowest-energy charged excitation. At $B = 8\,{\rm T}$, figure 3(a) (both axes are normalized to the Coulomb energy $E_{\rm c} = e^2/4\pi\varepsilon l_{\rm B}$, where $\varepsilon = 6.24\varepsilon_0$ and $l_{\rm B}$ is the magnetic length) shows $\Delta/E_{\rm c}$ versus $E_{\rm v}/E_{\rm c}$. The orange line near the crossing yields $s \approx 10$, evidencing multi-flip valley skyrmions; away from the crossing ($\eta > 0.01$), the olive line gives $\partial\Delta/\partial E_{\rm v} \approx 1$, i.e., single-particle excitations. Similar behaviors are observed at $B = 6\,{\rm T}$ but with a smaller skyrmion size of ~ 6. Both the skyrmion sizes and the transition from skyrmion excitations to single-particle excitations are consistent with the reported results in AlAs.[14,15] Whereas at $B = 4\,{\rm T}$, we find s reduces to ~ 1, indicating a reversion to the single-particle regime. This could be attributed to disorder and LL mixing, which we discuss later.

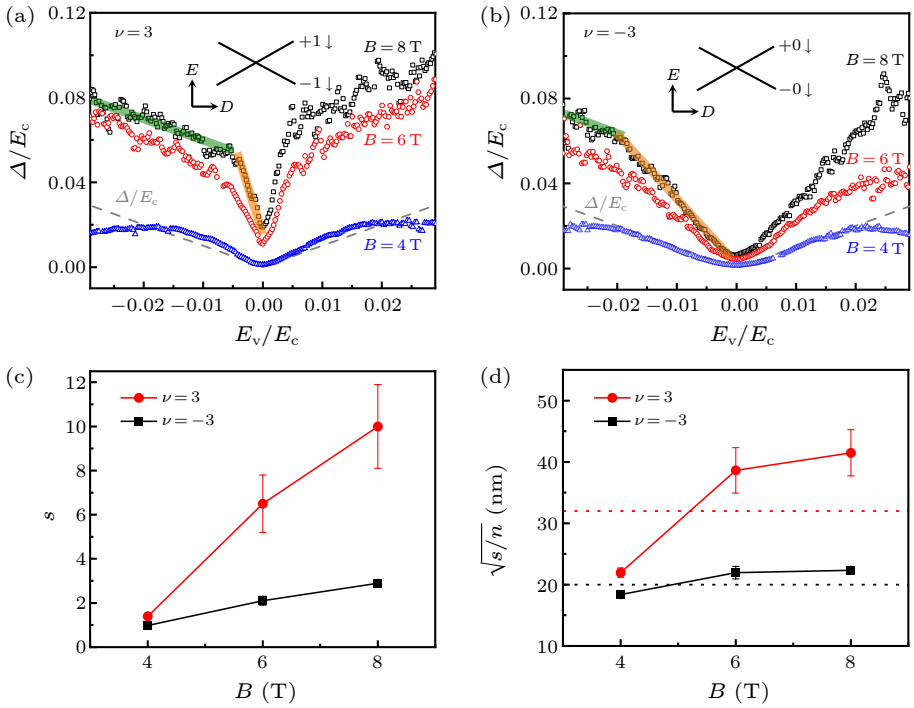

Fig. 3. Energy gap (Δ) of crossings at different magnetic fields for (a) $\nu = 3$ and (b) $\nu = -3$. Both axes are scaled to the Coulomb energy ($E_{\rm c} = e^2/4\pi\varepsilon l_{\rm B}$). Insets show valley flip with unchanged spin and orbital indices at $\nu = \pm 3$ crossings. Grey dashed lines in the plots denote the ideal gap from a single-particle picture. The evolution of energy gap around the crossing is consistent with a picture of valley skyrmions. The orange and olive lines are guides to the eye representing skyrmions ($s > 1$) and single-particle ($s = 1$) cases, respectively. (c) s (size of the valley skyrmions) and (d) $\sqrt{s/n}$ (inferred length scale of the skyrmion domain) versus B for $\nu = \pm 3$.

The evolution of s with magnetic field at a fixed filling [Fig. 3(c)] is consistent with a picture in which larger exchange energy and carrier density favor multi-flip excitations near the crossing. To connect this to a real-space description, $\sqrt{s/n}$ is used as a proxy for a characteristic skyrmion domain length scale [15] and plotted versus B in Fig. 3(d), where n is the carrier density at the corresponding filling. The resulting length scale is ∼32 nm (±10 nm) for $\nu = 3$, with only weak field dependence, suggesting that the underlying disorder landscape sets a nearly fixed spatial scale at a given filling.

Similar to $\nu = 3$, the $\nu = -3$ crossing involves a single-valley flip at fixed spin, but between $n = 0$ orbital rather than $n = 1$ as in the $\nu = 3$ case. The gaps and corresponding parameter values for $\nu = -3$ are summarized in Fig. 3(b) and included in Figs. 3(c) and 3(d). Over the range $B = 4$ T to 8 T, $\nu = -3$ shows the same overall field dependence as $\nu = 3$: $s \approx 1$ at $B = 4$ T, and $s > 1$ increasing with B at 6 T and 8 T, while the inferred length scale $\sqrt{s/n}$ remains nearly field independent [∼20 nm (±3 nm)]. However, at a given B, the absolute values of s and $\sqrt{s/n}$ are systematically smaller for $\nu = -3$. This quantitative difference may be linked to the different layer polarization and orbital structure of the $n = 0$ and $n = 1$ LL in BLG, and a full understanding will require further experimental and theoretical investigation.

The combined effects of disorder and LL mixing can now be distinguished across field regimes to explain the B dependence of the data. At low fields, the cyclotron gap is small and LL mixing—parameterized by $\kappa = E_c/\hbar\omega_c$ with $E_c \propto \sqrt{B}$ and $\hbar\omega_c \propto B$—is enhanced ($\kappa \propto 1/\sqrt{B}$), while disorder broadening can rival the LL spacing. Both effects suppress skyrmion excitations, [11,36] consistent with $s \approx 1$ at $B = 4$ T. At higher fields, larger gaps reduce mixing and mitigate disorder broadening, allowing multi-flip excitations to develop ($s > 1$ at $B = 8$ T and 6 T) while the inferred length scale remains set primarily by the disorder potential. Notably, the WSe_2/BLG/WSe_2 structure resides in an overall lower-κ regime than typical hBN-encapsulated graphene at the same B—owing to its higher effective dielectric environment and additional screening—which reduces the relative impact of LL mixing. This structural advantage helps to maintain a thermally activated gap at crossings and makes valley skyrmions resolvable in our device at comparatively low B and elevated temperatures. For completeness, measurements and analysis of valley skyrmions are also carried out for the middle crossing at $\nu = \pm 1$ (similar to the $\nu = \pm 3$ crossing). The corresponding results are presented in the Section V of the SM.

Beyond valley-only transitions, valley-orbital and valley-spin entangled pseudospin transitions also occur in our system at $\nu = \pm 2$ and $\nu = \pm 1$, respectively. Energy gaps Δ vs. D field at $B = 6$ T at $\nu = -2$ and $\nu = -1$ are shown in Figs. 4(a) and 4(b). In Fig. 4(a), the evolution of the gap near the $\nu = -2$ crossing resembles the $\nu = 3$ behavior, which could be considered as entangled pseudospin skyrmions. Another feature at $\nu = -2$ is that the energy gap between the two crossings greatly exceeds the predicted value of the LL spacing. The energy gap Δ vs. D field near $\nu = -1$ crossings in Fig. 4(b) shows violation of the single-particle model as well. With valley-orbital and valley-spin entangled pseudospin, these regimes involve competing anisotropies and require further study to clarify the excitation spectrum and pseudospin textures.

We close with a discussion of the applicability of the skyrmion framework to the present system. While other many-body effects such as enhanced valley splitting effect and valley-coherent effect can reproduce individual features, they do not account for the full set of dependencies on D field and B. In particular, the enhanced valley splitting effect itself does not account for a robust finite gap at exact degeneracy together with the two-regime slope behavior from $s > 1$ to $s \approx 1$. [25,28] The valley-coherent state does not preclude topological textures—indeed, valley-skyrmion-like textures have been imaged in a Kekulé intervalley-coherent QH ferromagnet. [21] We also note that similar resistance spike suppression has also been discussed in terms of domain-wall pinning in previous studies, [12,38–40] and the domain scenario may also account for the transport mechanism at ultralow temperature (below 150 mK) in the present system. However, our Arrhenius analysis performed in the higher temperature regime characterizes the energy cost of charged excitations above the QH ferromagnetic ground state rather than dissipation between domains. Taken together with prior skyrmion phenomenology and theoretical expectations for QH ferromagnets at small symmetry-breaking energy, our observations are naturally compatible with a valley-skyrmion interpretation.

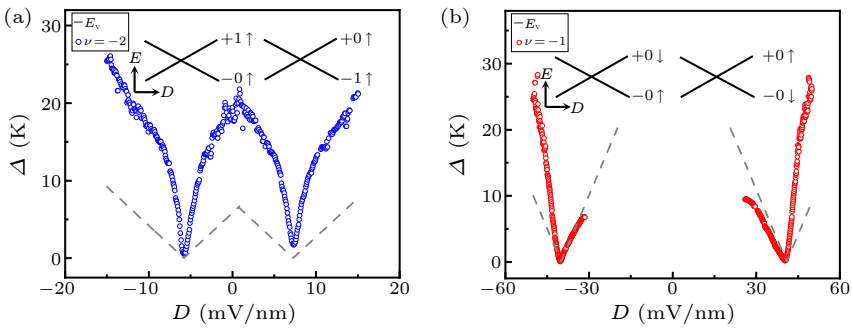

Fig. 4. Entangled pseudospin transitions and skyrmions. Energy gap (Δ) around (a) $\nu = -2$ and (b) $\nu = -1$ crossings versus D field at $B = 6$ T. Grey dashed lines denote the single-particle valley splitting energy. The insets show valley-orbital and valley-spin entangled pseudospin transitions at the crossings. The measured gaps deviate from the single-particle prediction in a manner consistent with skyrmion-like excitations.

4. Conclusion. In summary, we accessed isolated valley-only level crossings in the LLL using a WSe_2/BLG/WSe_2 heterostructure, where the long-range Coulomb interaction and LL mixing are expected to be suppressed, enabling precise mapping of the activation gaps. The evolution of the energy gaps at $\nu = \pm 3$ as functions of the out-of-plane D field and magnetic field, highly consistent with the results in AlAs QH systems, indicates the appearance of valley skyrmions. While transport results provide indirect evidence, direct probes of pseudospin textures would be valuable to further constrain alternative scenarios. Extending our measurement to fractional fillings would be a natural direction for exploring the robustness of skyrmions and complex spin/pseudospin textures in BLG.

Acknowledgements. We thank Ke Huang, Yang Liu and Xin Wan for discussions. The work at Peking University was supported by the National Key Research and Development Program of China (Grant No. 2021YFA1401900) and the National Natural Science Foundation of China (NSFC) (Grant No. 12141001). The work at Zhejiang University was supported by the NSFC (Grant Nos. 12374047 and U23A2076), the Fundamental Research Funds for the Central Universities (Grant No. 226-2025-00118), and the National Key Research and Development Program of China (Grant No. 2021YFA1401902 for Z.L.).

References

[1] Dieny B, Prejbeanu I L, Garello K, Gambardella P, Freitas P, Lehndorff R, Raberg W, Ebels U, Demokritov S O, Akerman J, Deac A, Pirro P, Adelmann C, Anane A, Chumak A V, Hirohata A, Mangin S, Valenzuela S O, Onbaşlı M C, d'Aquino M, Prenat G, Finocchio G, Lopez-Diaz L, Chantrell R, Chubykalo-Fesenko O, and Bortolotti P 2020 *Nat. Electron.* **3** 446
[2] Schaibley J R, Yu H, Clark G, Rivera P, Ross J S, Seyler K L, Yao W, and Xu X 2016 *Nat. Rev. Mater.* **1** 16055
[3] Nagaosa N and Tokura Y 2013 *Nat. Nanotech.* **8** 899
[4] Fert A, Reyren N, and Cros V 2017 *Nat. Rev. Mater.* **2** 17031
[5] Sampaio J, Cros V, Rohart S, Thiaville A, and Fert A 2013 *Nat. Nanotechnol.* **8** 839
[6] Liu Y, Lei N, Wang C, Zhang X, Kang W, Zhu D, Zhou Y, Liu X, Zhang Y, and Zhao W 2019 *Phys. Rev. Appl.* **11** 014004
[7] Okamura Y, Kagawa F, Mochizuki M, Kubota M, Seki S, Ishiwata S, Kawasaki M, Onose Y, and Tokura Y 2013 *Nat. Commun.* **4** 2391
[8] Barrett S E, Dabbagh G, Pfeiffer L N, West K W, and Tycko R 1995 *Phys. Rev. Lett.* **74** 5112
[9] Schmeller A, Eisenstein J P, Pfeiffer L N, and West K W 1995 *Phys. Rev. Lett.* **75** 4290
[10] Maude D K, Potemski M, Portal J C, Henini M, Eaves L, Hill G, and Pate M A 1996 *Phys. Rev. Lett.* **77** 4604
[11] Shukla S P, Shayegan M, Parihar S R, Lyon S A, Cooper N R, and Kiselev A A 2000 *Phys. Rev. B* **61** 4469
[12] Muraki K, Saku T, and Hirayama Y 2001 *Phys. Rev. Lett.* **87** 196801
[13] Ma M K, Wang C, Chung Y J, Pfeiffer L N, West K W, Baldwin K W, Winkler R, and Shayegan M 2022 *Phys. Rev. Lett.* **129** 196801
[14] Shkolnikov Y P, Misra S, Bishop N C, De Poortere E P, and Shayegan M 2005 *Phys. Rev. Lett.* **95** 066809
[15] Gokmen T and Shayegan M 2010 *Phys. Rev. B* **81** 115336
[16] Padmanabhan M, Gokmen T, and Shayegan M 2010 *Phys. Rev. Lett.* **104** 016805
[17] Young A F, Dean C R, Wang L, Ren H, Cadden-Zimansky P, Watanabe K, Taniguchi T, Hone J, Shepard K L, and Kim P 2012 *Nat. Phys.* **8** 550
[18] Zhou H, Polshyn H, Taniguchi T, Watanabe K, and Young A F 2019 *Nat. Phys.* **16** 154
[19] Yu J, Foutty B A, Kwan Y H, Barber M E, Watanabe K, Taniguchi T, Shen Z X, Parameswaran S A, and Feldman B E 2023 *Nat. Commun.* **14** 6679
[20] Pandey V, Ghosh P, Pal R, Paul S, B A M, Watanabe K, Taniguchi T, Nath Pal A, and Kochat V 2025 arXiv:2503.20392 [cond-mat.mes-hall]
[21] Liu X, Farahi G, Chiu C L, Papic Z, Watanabe K, Taniguchi T, Zaletel M P, and Yazdani A 2022 *Science* **375** 321
[22] Hunt B M, Li J I A, Zibrov A A, Wang L, Taniguchi T, Watanabe K, Hone J, Dean C R, Zaletel M, Ashoori R C, and Young A F 2017 *Nat. Commun.* **8** 948
[23] Li J I A, Tan C, Chen S, Zeng Y, Taniguchi T, Watanabe K, Hone J, and Dean C R 2017 *Science* **358** 648
[24] Li J, Tupikov Y, Watanabe K, Taniguchi T, and Zhu J 2018 *Phys. Rev. Lett.* **120** 047701
[25] Huang K, Fu H, Hickey D R, Alem N, Lin X, Watanabe K, Taniguchi T, and Zhu J 2022 *Phys. Rev. X* **12** 031019
[26] Xiang F, Gupta A, Chaves A, Krix Z E, Watanabe K, Taniguchi T, Fuhrer M S, Peeters F M, Neilson D, Milosevic M V, and Hamilton A R 2023 *Nano Lett.* **23** 9683
[27] Chuang Y W, Li J, Fu H, Watanabe K, Taniguchi T, and Zhu J 2019 *Phys. Rev. B* **100** 195402
[28] Wang D, Che S, Cao G, Lyu R, Watanabe K, Taniguchi T, Lau C N, and Bockrath M 2019 *Nano Lett.* **19** 7028
[29] Island J O, Cui X, Lewandowski C, Khoo J Y, Spanton E M, Zhou H, Rhodes D, Hone J C, Taniguchi T, Watanabe K, Levitov L S, Zaletel M P, and Young A F 2019 *Nature* **571** 85
[30] Tiwari P, Srivastav S K, Ray S, Das T, and Bid A 2020 *ACS Nano* **15** 916
[31] Papic Z, Thomale R, and Abanin D A 2011 *Phys. Rev. Lett.* **107** 176602
[32] Veyrat L, Déprez C, Coissard A, Li X, Gay F, Watanabe K, Taniguchi T, Han Z, Piot B A, Sellier H, and Sacépé B 2020 *Science* **367** 781
[33] Laturia A, Van de Put M L, and Vandenberghe W G 2018 *npj 2D Mater. Appl.* **2** 6
[34] Hou Y, Wang G, Ma C, Feng Z, Chen Y, and Filleter T 2022 *Mater. Charact.* **193** 112313
[35] Kedves M, Szentpéteri B, Márffy A, Tóvári E, Papadopoulos N, Rout P K, Watanabe K, Taniguchi T, Goswami S, Csonka S, and Makk P 2023 *Nano Lett.* **23** 9508
[36] Cooper N R 1997 *Phys. Rev. B* **55** R1934
[37] Fertig H A, Brey L, Côté R, MacDonald A H, Karlhede A, and Sondhi S L 1997 *Phys. Rev. B* **55** 10671
[38] Brey L and Tejedor C 2002 *Phys. Rev. B* **66** 041308(R)
[39] Jungwirth T and MacDonald A H 2001 *Phys. Rev. Lett.* **87** 216801
[40] De Poortere E P, Tutuc E, Papadakis S J, and Shayegan M 2000 *Science* **290** 1546